Vol. 531: 43–61, 2015
doi: 10.3354/meps11325

MARINE ECOLOGY PROGRESS SERIES
Mar Ecol Prog Ser

Published July 2

Impact of phytoplankton size and physiology on particulate optical properties determined with scanning flow cytometry

Malcolm N. McFarland*, Jan Rines, James Sullivan, Percy Donaghay

University of Rhode Island, Graduate School of Oceanography, 215 South Ferry Road, Narragansett, RI 02882, USA

ABSTRACT: Layers and patches of phytoplankton at sub-meter scales in the vertical dimension and kilometer scales in horizontal dimensions are common features in the coastal ocean. These heterogeneous distributions of cells are fundamental to their population dynamics and the function of pelagic ecosystems. To better understand biological processes at these small scales, methods were developed to assess phytoplankton community composition and physiological characteristics based on high-resolution, *in situ* optical measurements. Scanning flow cytometry of discrete samples was used to determine the effects of phytoplankton and non-algal particle abundance, size, and pigment content on the spectral shape and relative magnitude of particulate attenuation, absorption, scatter, and backscatter coefficients. The slope of particulate attenuation varied with phytoplankton size and morphology, the slope of particulate absorption and the ratio of scatter to absorption varied primarily with cellular pigment content, and the backscatter ratio varied primarily with the relative abundance of non-algal particles. Determination of particle and phytoplankton characteristics from optical measurements over small spatial and temporal scales was tested with 2 independent high-resolution data sets collected from an *in situ* autonomous profiling system. Comparison of these high-resolution optical data with flow cytometric sample analyses generally agreed with the previously determined relationships but suggest that complex morphology of large colonial diatoms may result in higher than expected particulate attenuation slopes. High-resolution data revealed variations in community size structure and physiology that would be difficult to visualize with discrete samples or measures of total chlorophyll concentration.

KEY WORDS: Phytoplankton composition · Optical properties · Flow cytometry · Small scale

INTRODUCTION

It is well established that marine phytoplankton communities can vary considerably over very small spatial (decimeter) and temporal (minutes) scales (Cassie 1963, Haury et al. 1978, Derenbach et al. 1979, Bjørnsen & Nielsen 1991, Donaghay et al. 1992, Cowles et al. 1998, Rines et al. 2010). In the ocean, this structure is often observed as patches or thin layers that can contain a large proportion of chlorophyll biomass and that persist over time scales important to phytoplankton growth, mortality and life history (Dekshenieks et al. 2001, McManus et al. 2003, Sullivan et al. 2010b). Variations in distribution and abundance over small scales, therefore, are fundamental to the ecology of planktonic organisms and to the function of marine pelagic ecosystems. This heterogeneous distribution of organisms is a result of their interactions with physical, chemical, and biological ecosystem components (Durham & Stocker 2012). The ecological processes that occur within and around small-scale structures can be important to the establishment of harmful algal blooms (Donaghay & Osborn 1997, Smayda & Reynolds 2001, Rines et al. 2002), trophic interactions (Nielsen et al. 1990, Menden-Deuer 2008, Benoit-Bird et al. 2009, Greer

*Corresponding author: malcolm@my.uri.edu

et al. 2013), biochemical cycling (Sieburth & Donaghay 1993, Hanson & Donaghay 1998), sexual reproduction (Peperzak 2006), and community assembly, succession, and diversity (Smayda & Reynolds 2001, Reynolds 2006).

Technological developments over the past several decades have enabled *in situ* analysis of natural phytoplankton communities with increasing resolution over decreasing spatial and temporal scales. High-resolution methods targeting phytoplankton typically use optical measurements of absorption, attenuation, scattering or fluorescence to detect and map small-scale structure (Derenbach et al. 1979, Cowles & Desiderio 1993, Twardowski et al. 1999). Modern optical instrumentation can routinely collect data at high rates (>1 Hz) and can be deployed on a variety of profiling, towed, moored, or autonomous platforms (Babin et al. 2005, Holliday et al. 2009, Sullivan et al. 2010a). While these data are often used to infer total phytoplankton biomass, a better understanding of ecological processes over small scales could be obtained from optical parameters that respond to variation of phytoplankton characteristics such as cell size, shape, or physiology (Stemmann & Boss 2012).

Theoretical and empirical bio-optical studies have shown the shape and relative magnitude of particulate absorption (a_p), scattering (b_p), and attenuation (c_p) coefficient spectra are determined by particle size, morphology, and complex refractive index (Morel & Bricaud 1986, Sathyendranath et al. 1987). These particle characteristics can vary significantly among phytoplankton taxa and with their physiology (Bricaud et al. 1983, Spinrad & Yentsch 1987, Ackleson et al. 1988, Stramski & Reynolds 1993). Intracellular pigment packaging can flatten and decrease the slope of the a_p spectrum while reducing the absorption efficiency of cells (Duyens 1956, Kirk 1975, Ciotti et al. 2002). The slope of a_p spectra between 488 and 532 nm may also increase as the ratio of photoprotective to photosynthetic carotenoids increases (Eisner et al. 2003). The ratio of scattering to absorption (b_p:a_p) can vary among particle types and with intracellular carbon and pigment concentrations (Stramski & Morel 1990, Sosik et al. 2001). The proportion of light scattered in the backward direction (b_{bp}:b_p) is low for large particles and particles with low refractive index. Smaller particles or those with high refractive index have a higher b_{bp}:b_p (Twardowski et al. 2001, Sullivan et al. 2005). The exponential slope of the c_p spectrum is high for suspensions dominated by very small particles such as picoplankton or suspended sediments, and closer to zero for suspensions with abundant large particles such as diatom or dinoflagellate cells (Kitchen et al. 1982, Boss et al. 2001). Owing to their dependence on particle characteristics, these optical parameters convey ecologically important information about the composition and physiology of phytoplankton communities in the ocean.

Previous work in multiple different marine ecosystems suggests that particle characteristics are important to the bulk inherent optical properties (IOPs) of ocean waters that can be measured *in situ* with high resolution (Babin et al. 2003, Bricaud et al. 2004, Eisner & Cowles 2005, Sullivan et al. 2005). However, few field studies have directly measured individual phytoplankton and non-algal particle characteristics to determine their influence on bio-optical parameters and test the predictive capabilities of optical data. Iturriaga & Siegel (1989) used microspectrophotometric measurements of individual particles to show that particles from 3 to ~50 µm in size account for nearly all relevant absorbing particles and phytoplankton account for 50 to 70% of a_p at 440 nm in North Atlantic mesotrophic waters. They also found substantial variation in the absorption spectra of individual phytoplankton and non-algal particles, and variations in particle size and absorption efficiency with depth. However, their methods were labor-intensive and limited to approximately 50 particles for each water sample. In a study conducted in New England continental shelf waters, Green et al. (2003) used flow cytometry to show that bulk IOPs were highly dependent on the abundance, size, and complex refractive index of different plankton and particle groups. While focusing primarily on larger scales, the authors documented significant variation in phytoplankton optical cross-sections and complex refractive indexes between spring and summer communities and with depth. They also found that eukaryotic phytoplankton account for the majority of particulate absorption and scattering, mineral and detrital particles contribute most to backscattering, and small photosynthetic prokaryotes make only small contributions (<14%) to bulk IOPs. A previous study in Monterey Bay, California, USA, found that variation of phytoplankton community taxonomic composition and characteristics over small scales, determined with microscope-based observations and cell counts, were correlated with changes in the relative magnitude and spectral shape of a_p, b_p, and c_p coefficient spectra (M. McFarland unpubl.). The slopes of particulate attenuation and absorption spectra varied most with community composition, suggesting that the size distribution and pigment

content of cells are optically important phytoplankton characteristics that differentiate communities. That study, however, clearly demonstrated the need for quantitative measurements of cell size, pigment content, and non-algal particles. Collectively, these previous studies suggest that particulate optical properties can provide valuable biological information about phytoplankton community composition and characteristics when measured at high resolutions in the ocean.

In the present study, conducted in the coastal fjord of East Sound, Washington, USA, the influence of natural phytoplankton and non-algal particle characteristics on particulate IOPs was assessed and the ability of *in situ* optical measurements to determine phytoplankton community characteristics with high resolution over small spatial and temporal scales was tested. A scanning flow cytometer was used to directly measure abundance, size, and fluorescence of phytoplankton cells and non-algal particles in discrete seawater samples. The accuracy of the flow cytometry data was validated with independent field- and laboratory-based experiments. The relationships between particle characteristics and corresponding measurements of the b_p:a_p, a_p slope, c_p slope, and b_{bp}:b_p parameters were determined with a redundancy analysis. Based on these relationships, an independent, high-resolution optical data set collected with an autonomous profiler was used to infer phytoplankton and non-algal particle characteristics over small scales. Finally, these inferences were tested by comparison with the particulate composition of discrete samples determined with scanning flow cytometry. The methods employed in this study enabled visualization of phytoplankton community characteristics with high resolution and can be used to better understand the ecological dynamics of phytoplankton populations and the processes that determine the abundance of different taxa over small scales.

MATERIALS AND METHODS

This study was conducted in East Sound, a small fjord located in the northwest corner of Washington state at 48.7°N latitude. It is approximately 13 km in length, 2 km wide, oriented in a north-northwest direction and open at the southern end. The sound is 30 to 40 m deep on average with narrow topographical constraints and a partial shallow sill at the southern mouth. Currents and mixing are primarily driven by wind and tides. When mixing is not intense, East Sound often develops a complex layered structure. Multiple distinct water masses can be stacked on top of each other with significant differences in phytoplankton community composition (Dekshenieks et al. 2001, Rines et al. 2002, McManus et al. 2003). This layered water column structure makes East Sound an excellent system in which to capture large amounts of biological and optical variation.

Ship-based optical profiles and corresponding samples were collected between 14 and 26 May 2009 and between 8 and 20 May 2010. Sample depths were selected based on ship-based optical profile data available in real time and samples were immediately analyzed on board the ship with microscopy and scanning flow cytometry. Ship-based profiles and samples were collected from a wide range of locations throughout the sound to capture the full range of variability in community structure and optical properties. High-temporal resolution optical profiles (every 1 or 2 h) were also collected from an autonomous profiling instrument package moored at one location in the northern half of the sound over a shorter time period than ship-based profiling and sample collection (from 20 to 26 May 2009 and from 11 to 15 May 2010). To acquire samples that could be directly compared to autonomous profiler data, ship-based profiling and sample collection was occasionally conducted adjacent to the autonomous profiler.

Optical data from ship-based profiles were compared with flow cytometric analyses using multivariate statistical methods (cluster analysis and redundancy analysis) to determine relationships between particle characteristics and bulk optical properties. These relationships were used to interpret high-resolution optical data collected from the autonomous profiler. To test relationships between optical data and particle characteristics, high-resolution optical data were compared to flow cytometry data from a small subset of samples collected adjacent to the autonomous profiler.

Ship-based optical profiles

Optical data for comparison with discrete samples were collected from multiple locations throughout the sound with a ship-based profiling instrument package. Instruments included a WET Labs ac-9 (2009) or ac-s (2010) absorption and attenuation meter, a WET Labs ac-9 fitted with a 0.2 µm filter at the intake to measure absorption by dissolved substances, a SeaBird Electronics SBE-25 CTD, a WET Labs WETStar chlorophyll fluorometer, and a WET Labs

ECO Volume Scattering Function (VSF) 532 nm scatter sensor. During 2010 the profiler also included a WET Labs Colored Dissolved Organic Matter (CDOM) fluorometer. The buoyancy of the optical instrument package was adjusted to be slightly negative and, during data collection, was allowed to descend freely through the water column, decoupled from ship motion (Donaghay et al. 1992). Profiles were conducted in duplicate to ensure the accuracy of measurements and stability of the local water column structure.

Absorption and attenuation meters were calibrated before, during and after each field project with 0.2 µm filtered de-ionized water from a Barnstead E-pure water purification system. Optical data were corrected for the effects of temperature and salinity according to the methods of Twardowski et al. (1999) and Sullivan et al. (2006). Scattering errors in the ac-9 and ac-s meters were corrected using the proportional correction algorithm of Zaneveld et al. (1994). Use of other scattering correction methods, including subtraction of particulate absorption at 715 nm from all wavelengths and the proportional+ method of Röttgers et al. (2013), did not have an effect on subsequent statistical analyses. The coefficients a_p and c_p were calculated by subtracting dissolved absorption (a_g), measured with the 0.2 µm filtered ac-9, from total absorption (a_{pg}) and attenuation (c_{pg}), measured with the unfiltered ac-9 or ac-s meters. An in-line flow sensor was used to compensate for the slower flow rate through the filtered ac meter by applying a time delay based on an experimentally determined linear fit of delay to flow meter voltage. To match the higher spectral resolution of the ac-s meter used during 2010, the dissolved absorption spectrum was interpolated by fitting to measured values, an equation of the form $a_g(\lambda) = s\lambda^{-\gamma}$, where λ is the wavelength, γ is the exponential slope, and s is a scale factor. The coefficient b_p was calculated as the difference between the particulate absorption and attenuation coefficients, $b_p = c_p - a_p$. Values of b_{bp} at 532 nm were calculated from the ECO VSF data integrated over all 3 angles, after each angle was calibrated according to a weighting function as described in Sullivan et al. (2013).

Adaptive sampling

Optical profiles were conducted immediately prior to water sample collection and target sample depths were selected based on total phytoplankton biomass inferred from optical data available in real time. Depths were selected to capture the maximum amount of variation of biomass throughout the water column in the most efficient manner possible. At each profiling station, samples were generally collected from 2 or 3 depths where total absorption and chlorophyll fluorescence exhibited minimum and maximum values. This adaptive sampling procedure ensured that thin layers of phytoplankton were accurately sampled and the full range of phytoplankton biomass and optical variation throughout the water column was captured at each station. Samples were collected with a ~2 l, hand-deployed, Ruttner-type water sampler (KC Denmark) on a graduated line. Sub-samples (~20 ml) were used for immediate flow cytometric analysis on board the ship. For qualitative analysis of communities and species identification, phytoplankton cells and colonies in collected samples were immediately viewed and recorded on the ship with a compound microscope equipped with a video camera. Sub-samples for video microscopy were gently concentrated with a 20 µm Nitex mesh screen. In addition, 250 ml of each sample was preserved with 1% formalin and 1% glacial acetic acid for later analysis in the lab. Preserved samples were used to validate flow cytometry data (see 'Scanning flow cytometry').

Scanning flow cytometry

A CytoSense scanning flow cytometer (CytoBuoy b.v.) was used aboard the ship to measure the size, concentration, light scatter, and chlorophyll fluorescence of phytoplankton cells and non-algal particles in samples immediately after collection. This instrument has a wide flow path that can accommodate particles up to 800 µm in width. The CytoSense records a scan (0.5 µm resolution) of the light scattered and fluoresced by particles as they pass individually through the incident laser beam at a fixed speed (Fig. 1). Descriptive particle parameters such as total light scatter, total fluorescence, and length are computed for each particle from scan data. Particles that are elongate in shape tend to align lengthwise along the axis of flow and length measurements therefore represent maximum particle dimensions rather than spherical equivalent diameters (Fig. 1A,B). For each sample, the volume of fluid analyzed is recorded and used to calculate particle concentrations. Sample volumes generally ranged from several hundred microliters to several milliliters, depending on particle concentration. The CytoSense flow cytometer used in this study was equipped with a 488 nm blue laser and

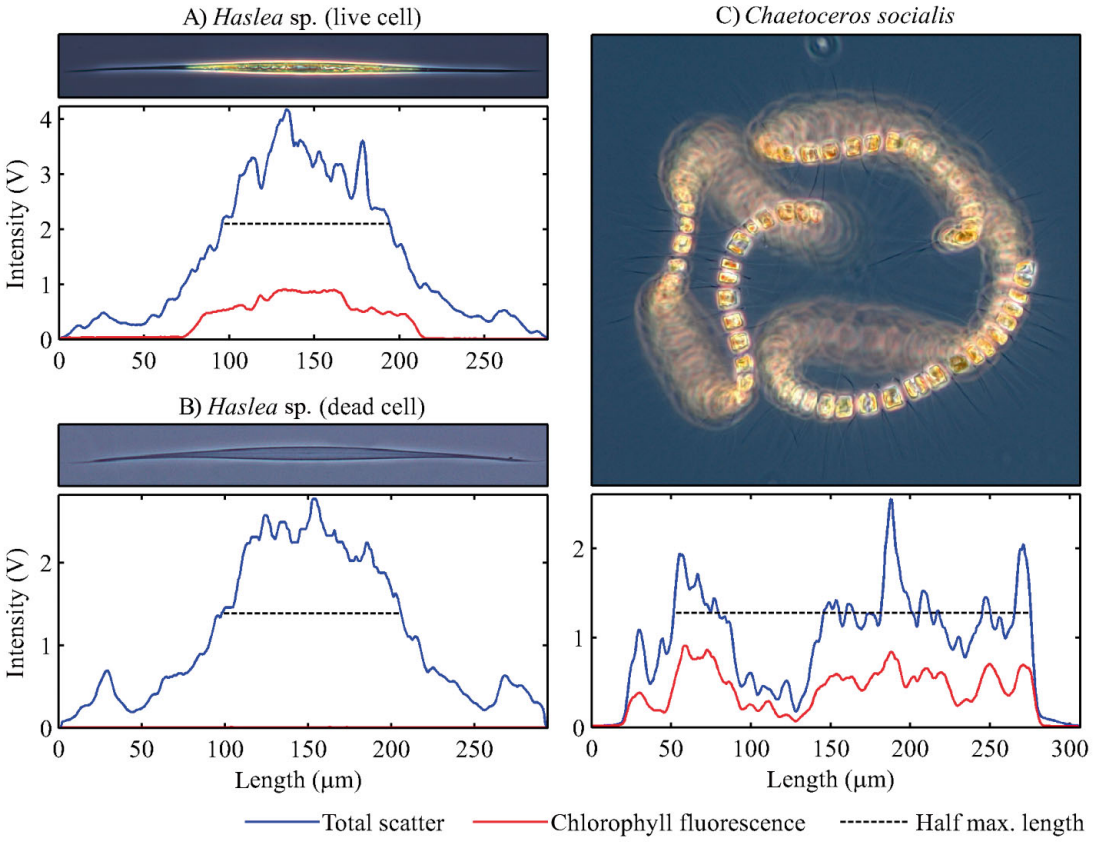

Fig. 1. Examples of several phytoplankton cells and corresponding scan data from the CytoSense flow cytometer. (A) Image of live *Haslea* sp. cell above corresponding CytoSense scan. (B) Image and scan of empty *Haslea* sp. frustule. Note lack of chlorophyll fluorescence. (C) Image and corresponding scan of live *Chaetoceros socialis* colony. Dashed lines indicate particle length determined from scan data by CytoClus software

detectors for forward scatter, side scatter, and fluorescence at green (515 to 565 nm), yellow (565 to 595 nm), orange (595 to 664 nm), and red (>664 nm) wavelengths. Detector gain settings and trigger levels were adjusted using natural samples and phytoplankton cultures to ensure adequate signal strength and detection of cells as small as 2 µm (e.g. *Synechococcus*), and to avoid saturation by large dinoflagellates or colonial diatoms (e.g. *Chaetoceros*) that are common in East Sound. To ensure comparable results, gain settings and trigger levels were kept consistent for all samples within each year, but were increased slightly in 2010 to improve detection of the smallest observable particles (e.g. bacteria). Alignment and performance of detectors was checked daily by running a broad-spectrum fluorescent 2.5-µm-diameter bead standard (Molecular Probes, AlignFlow beads).

The standard algorithm in the CytoBuoy CytoClus analysis software (version 3.0) calculates particle length from scan width at half-maximum, with a correction for particles smaller than the focused beam height. Although this algorithm worked well for small single cells, it was found to be inaccurate for large particles such as pennate diatoms or *Chaetoceros* spp. colonies that had low signal intensity near the ends of scans. Examples of lengths determined by the standard algorithm are shown as dashed lines in Fig. 1. For these large cells and colonies, total scan length was a more accurate determination of actual particle length. A modified algorithm was developed to calculate length according to scan width at a fraction of scan height that was dependent on total integrated forward scatter. For small particles, this new algorithm produced a length measurement that was nearly equivalent to the standard algorithm based on scan width at half-maximum. For large particles, the algorithm produced a length that was nearly equivalent to the total scan length. The algorithm used a generalized logistic function of the form:

$$f = 0.594 + \frac{0.01 - 0.594}{\left(1 + 0.001e^{-2.92(t-3.415)}\right)^{1000}} \quad (1)$$

where f is the fraction of scan height at which length should be determined and t is the base 10 log of the integrated forward scatter scan. In Eq. (1), the values 0.594 and 0.01 represent the highest and lowest possible fraction of scan height at which length should be determined. The value 3.415 represents the log of integrated forward scatter at the mid-point of the transition between the smallest and largest scan height fractions, and the value 2.92 represents the slope of this transition. These parameters were determined by unconstrained nonlinear optimization using the 'fminsearch' function in Matlab (The Mathworks). The procedure found parameter values that minimized the length measurement error of 6 bead size standards (Duke Scientific polymer microspheres) with diameters of 2.7, 9.7, 14.6, 20, 30.1, and 69.9 µm. Length measurements were then recalculated based on this optimized algorithm for scan data from all collected samples.

The accuracy of CytoSense concentration measurements was tested by comparison with manual microscope-based cell counts of a subset of samples collected during 2009 and 2 uni-algal phytoplankton cultures. Field samples contained an abundant population of the large pennate diatom *Haslea* sp., which was easily identified in the microscope and in CytoSense data due to its consistent size and shape. A culture of this taxon, isolated from East Sound in 2011, and a culture of the dinoflagellate *Akashiwo sanguinea*, isolated from Grays Harbor, Washington, USA, were also used to test CytoSense cell concentration measurements. Manual microscope-based cell counts of preserved field samples and cultures were conducted in the lab on a Nikon Eclipse E800 compound microscope using a 10× objective and phase contrast illumination. Cells were counted in a 0.1 ml Palmer-Maloney or 1 ml Sedgewick-Rafter chamber, depending on concentration.

The accuracy of CytoSense length measurements was tested for 4 uni-algal cell cultures by comparison with automated image analysis using a FlowCAM imaging particle analyzer. Selected species varied in size from approximately 10 µm to nearly 1 mm and included *Teleaulax amphioxeia* (Cryptomonadacea), *Akashiwo sanguinea* (Dinophyceae), *Chaetoceros socialis* (Bacillariophyceae), and *Chaetoceros eibenii* (Bacillariophyceae). Cultures were isolated from Narragansett Bay, Rhode Island; East Sound (*C. eibeneii*), or Grays Harbor, Washington, USA (*A. sanguinea*), and grown in L1 seawater medium (Guillard & Hargraves 1993) with a 12 h light:12 h dark cycle at 15°C. *A. sanguinea* and *T. amphioxeia* were grown in L1 medium without enrichment of silicon and diatoms were grown in lower strength L1/5 medium. To promote proper morphology of large colonial diatoms and prevent settling, cells were grown in 10 l tanks equipped with motorized stir bars to generate moderate levels of turbulence (Sullivan & Swift 2003). Measurements from 6 replicate tanks for each species were acquired while cells were in exponential growth phase.

Particle length, forward scatter, side scatter, chlorophyll fluorescence, and phycoerythrin fluorescence were used to classify particles into separate types. Classification was performed by manually defining parameter value ranges (gates) for different particle types on scatter plots of length vs. maximum red fluorescence, maximum forward scatter vs. maximum side scatter, and maximum red vs. maximum yellow fluorescence. Identifiable particle types included non-algal particles (without chlorophyll fluorescence), picoplankton-sized (~1 to 2 µm) *Synechococcus*, nanoplankton-sized (2 to 20 µm) photosynthetic eukaryotes, microplankton-sized (>20 µm) diatoms and dinoflagellates, nano- and microplankton sized cells with phycoerythrin (e.g. cryptomonads and *Dinophysis* spp.), and nano- and microplankton-sized dead algal cells. Dead cells were distinguished from live cells and non-algal particles by having very low residual chlorophyll fluorescence, but length and scatter characteristics similar to live cells.

Data analysis

For comparison with flow cytometry data, optical data were extracted from ship-based profiles collected at the same location, depth, and time as the samples. For each sample, 4 optical parameters that describe the shape and relative magnitude of a_p, c_p, and b_p spectra were calculated. These included the ratio of b_p at 555 nm to a_p at 676 nm (b_p:a_p), the spectral slope of the a_p coefficient between 488 and 532 nm, the spectral slope of c_p, and the ratio of b_{bp} to b_p at 532 nm (b_{bp}:b_p). Wavelengths for b_p:a_p were chosen to coincide with the peak scattering signal and the long-wavelength chlorophyll absorption peak to minimize the influence of absorption by non-algal particles. The a_p slope was calculated according to Eisner et al. (2003) as:

$$a_p\,\text{slope} = -\frac{a_{p488} - a_{p532}}{a_{p676}(488 - 532\,\text{nm})} \quad (2)$$

Note that Eisner et al. report the a_p slope as a negative value and we report this slope as a positive value to maintain consistency with conventions for

the c_p slope. The slope of c_p was determined between 412 and 650 nm by fitting an equation of the form $c_p(\lambda) = k\lambda^{-\gamma}$, where λ is the wavelength, γ is the exponential slope of the spectrum, and k is a scale factor (Twardowski et al. 2001, Boss et al. 2001). The equation was fitted using unconstrained nonlinear optimization to minimize the sum of squared errors between modeled and measured values of c_p. The backscatter ratio (b_{bp}:b_p) at 532 nm was calculated from b_{bp} measured with the ECO VSF and b_p measured with the ac-9 or ac-s, both at 532 nm.

A percent scatter distribution based on scanning flow cytometry data was used to characterize the particulate composition of samples. We used scatter, rather than particle concentration, to account for differences in particle cross-sectional area that determine their impact on bulk absorption, scattering, and attenuation coefficients (Morel & Bricaud 1986). For every sample, flow cytometry data for each of the 6 particle types was binned according to length into 50 logarithmically sized bins between 1 µm and 2 mm. This resulted in 300 categories of particle (50 sizes of each type) for which the percentage of total particle scatter was calculated. For each particle, scatter was calculated as the sum of the integrated forward scatter and side scatter scan data. The total scatter percentage was calculated as the sum of scatter for all particles of a given type in a size bin normalized by the sum of total scatter for all particles in the sample.

Hierarchical cluster analysis and redundancy analysis were used to determine the relationship between the particulate composition of samples and their corresponding optical properties. These analyses were conducted separately for each year due to differences in flow cytometer gain settings between years, which may have affected particle detection and classification. Gain settings were consistent for all samples within each year to ensure comparable data. The percentage of particle scatter by all 300 categories was used to cluster samples into 4 groups in each year. Hierarchical cluster analyses (complete linkage method) were based on a Bray-Curtis distance matrix and computed with the Matlab statistics toolbox version 8.0. Similarity profile tests were used to determine the distance at which the resulting dendrograms should be cut to produce compositionally distinct groups of samples. Dendrograms were subdivided at a fixed distance above which similarity profile tests could confirm significant structure ($p < 0.01$) for all groups (Clarke et al. 2008). This resulted in 4 clusters of samples in each year. Means for each cluster were determined by averaging percent scatter distributions and optical parameters among all samples in each community. Similarity profile tests were performed with the Fathom toolbox for Matlab (Jones 2012) using 10^4 iterations. Redundancy analysis is a multivariate statistical ordination technique similar to principal components analysis but with the ability to model linear relationships among 2 sets of variables (Zuur et al. 2007). It is a constrained method similar to canonical correspondence analysis that displays only the variation in one set of variables (i.e. flow cytometry data) that can be explained by another set of constraining variables (i.e. optical data). Redundancy analysis was performed with the 'vegan' package for the R statistical computing environment (Oksanen et al. 2013). Redundancy analyses were based on the same 300 categories of percent scatter data used for cluster analyses and measurements of the 4 optical parameters b_p:a_p, a_p slope, c_p slope, and b_{bp}:b_p corresponding to each sample.

High-resolution autonomous profiles

High-spatial and -temporal resolution optical data were collected with an Ocean Response Coastal Analysis System (ORCAS) autonomous vertical profiler (Donaghay 2003, Babin et al. 2005, Sullivan et al. 2005, Sullivan et al. 2010a) moored in the upper sound from 20 to 26 May 2009 and from 11 to 15 May 2010. This system is equipped with a programmable submersible winch anchored to the sea floor, floats to provide positive buoyancy, batteries, a data logger, and a radio system to transmit collected data to a receiving station. The instrument payload included a WET Labs ac-9 absorption and attenuation meter, a SeaBird Electronics SBE49 CTD, a WET Labs WETstar chlorophyll fluorometer, a WET Labs ECO VSF 3-angle backscatter sensor (532 nm), and a WET Labs CDOM fluorometer. The system collected profiles at an ascent rate of ~3 cm s^{-1}, resulting in data with a vertical spatial resolution of ~1 cm. Profiles were conducted hourly in 2010 and every 2 h in 2009. The ac-9 meter was calibrated before and after deployment and corrections for temperature, salinity, and backscatter errors were applied to data as with the ship-based profiling system. To minimize noise and enhance the appearance of ecologically relevant distribution patterns, outliers were removed and data were smoothed over depth and time. Profiles were concatenated and linearly interpolated to 1 cm depths between approximately 1 and 20 m. Outliers greater than 3 standard deviations from the mean measured over a 40 cm depth interval and a 4 h time interval were removed and gaps were filled by linear

interpolation. Concatenated data were then smoothed by convolution using Gaussian kernels with standard deviations of 10 cm and 1 h. Data were plotted with a linearly interpolated color gradient. Chlorophyll concentrations were calculated from absorption spectra according to the methods of Sullivan et al. (2005) using a chlorophyll-specific absorption coefficient of 0.014 m^2 mg^{-1} typical for East Sound. Absorption-based chlorophyll concentrations were used to avoid the effects of fluorescence quenching by photo-inhibition that can happen in near-surface waters.

As the ORCAS profiler could not be equipped with a filtered ac meter, a_g was determined from measurements of CDOM fluorescence. A model of a_g based on CDOM fluorescence and depth was developed from a_g and CDOM fluorescence measurements acquired with the ship-based profiling package during 2010. The value of a_g at 412 nm was found to be linearly related to CDOM fluorescence according to:

$$a_g(412\ \text{nm}) = 0.0135F + 0.1806 \quad (3)$$

where F is CDOM fluorescence. The exponential slope (s) of the a_g spectrum was found to vary with depth according to:

$$s = 0.0008e^{-0.2334d} + 0.016 \quad (4)$$

where d is depth. These relationships determined the parameters used to calculate a_g spectra according to:

$$a_g(\lambda) = a_{g(412\ \text{nm})}e^{-s(\lambda - 412)} \quad (5)$$

where λ is wavelength and s is the spectral slope. Modeled a_g spectra were then subtracted from total attenuation spectra to determine a_p spectra, c_p spectra and c_p slope.

To test the association between optical parameters and particle characteristics, b_p:a_p, a_p slope, c_p slope, and b_{bp}:b_p derived from high-resolution data were compared to samples collected from 3 points during the time series from each year. Samples were analyzed with scanning flow cytometry to determine particle composition and characteristics as described above.

RESULTS

CytoSense validation

Particle concentrations determined by flow cytometry and manual microscope counts were linearly related (Fig. 2A). A model II least-squares linear fit to the log-converted data had an r^2 value of 0.97, indicating consistent precision over a wide range of cell densities. Cell concentrations determined with the flow cytometer were generally slightly lower than those determined manually for all samples, a result that appears exaggerated at lower cell densities on the log:log plot. Flow-cytometry-based cell concentrations for *Haslea* sp. cultures may also have been slightly underestimated due to excessive production of exopolymers, which could have caused cells to stick to each other and to sample tubing. Cell length measurements determined with the CytoSense flow cytometer were similar to those determined by

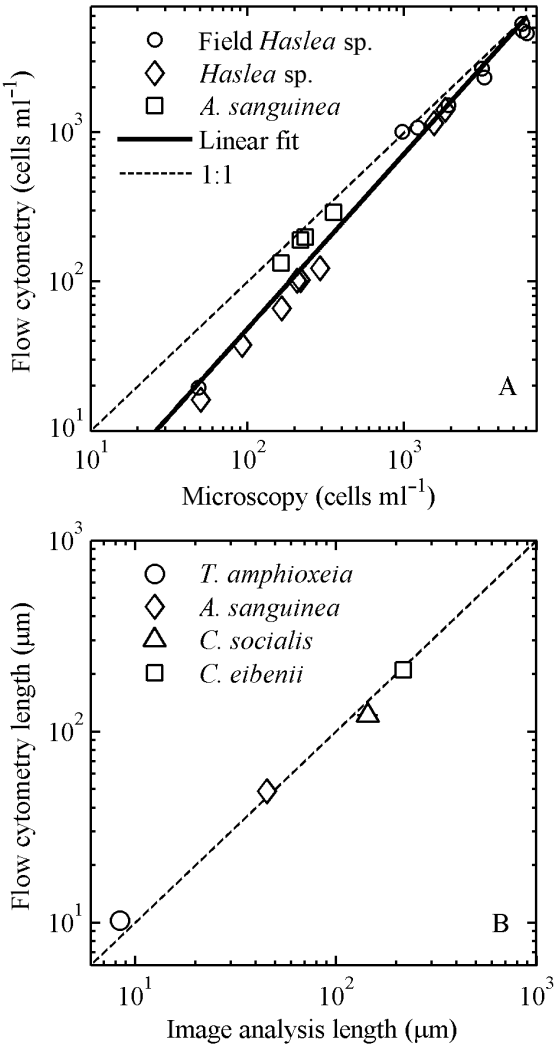

Fig. 2. (A) Comparison of phytoplankton cell concentrations determined by flow cytometry and manual, microscope-based cell counts. (B) Comparison of mean phytoplankton cell length measurements determined by scanning flow cytometry and automated image analysis for 4 different uni-algal cultures. Standard error bars are smaller than all symbols. Species: *Akashiwo sanguinea*; *Chaetoceros eibenii*; *Chaetoceros socialis*; *Teleaulax amphioxeia*

automated image analysis with a FlowCAM particle analyzer (Fig. 2B). CytoSense length measurements were slightly higher than FlowCAM measurements for the smallest cells (*Teleaulax amphioxeia*) and slightly lower than FlowCAM measurements for the larger *Chaetoceros socialis*.

Ship-based optical profiles and sample analyses

A total of 55 samples in 2009 and 61 samples in 2010 were acquired and analyzed. Microscopy of live samples collected during 2009 revealed a phytoplankton community dominated by an abundant population of a pennate diatom in the genus *Haslea* (Fig. 1A,B). During 2010, live microscopy revealed a phytoplankton community still dominated by diatoms, but with a greater diversity of species including multiple *Chaetoceros* (especially *C. socialis*, Fig. 1C) and a number of other colony-forming centric and pennate diatoms including *Dactyliosolen fragilissimus*, *Detonula pumila*, *Ditylum brightwellii*, *Eucampia zodiacus*, *Guinardia delicatula*, *Pseudo-nitzschia* spp., *Skeletonema* spp., *Rhizosolenia* spp., *Leptocylindrus danicus*, and *Thalassiosira* spp. These species represent a wide range of cell sizes, shapes, and modes of colony formation. Individual cells of these species could be as small as ~10 µm (e.g. *Skeletonema* spp.), whereas colonies of *C. socialis* or single cells of *Rhizosolenia* spp. could be several hundred micrometers in size. The morphology of the siliceous frustules for many of these diatoms was quite complex, with some species having long siliceous setae or interconnecting spines (e.g. *Chaetoceros* spp. and *Skeletonema* spp.) and others with patterns of pores or striations along the valve face (e.g. *Thalassiosira* spp., *Pseudo-nitzschia* spp., and *Haslea* sp.).

Approximately 1 ml of seawater and an average of 16589 particles were analyzed per sample with the scanning flow cytometer during 2009. Average sample volume and number of particles analyzed were increased during 2010 to 1.7 ml of seawater and 58681 particles per sample, to account for a lower overall concentration of phytoplankton and a more diverse phytoplankton community. During 2009, particles were classified as non-algal, eukaryotic cells containing phycoerythrin, live *Haslea* sp., dead *Haslea* sp., nanophytoplankton, or microphytoplankton. Despite initial efforts to calibrate detector gain settings and trigger levels prior to sample analyses, signal strength from picoplankton-sized cells was insufficient for accurate enumeration in most samples. However, despite their high abundance, these small cells accounted for a very small proportion of total scatter or fluorescence, most likely due to their small size or low refractive index. Low contributions of picophytoplankton-sized cells to total scatter were also found by Green et al. (2003). During 2010, gain settings were increased and trigger levels were decreased to ensure efficient detection of *Synechococcus*. Flow cytometer data collected during 2010 were classified as non-algal, eukaryotic cells with phycoerythrin, *Synechococcus*, nanophytoplankton, microphytoplankton, and dead cells.

Cluster analyses based on the particulate composition of samples identified 4 distinct communities in each year (Fig. 3). Similarity profile analyses confirmed the significance of all clusters ($p < 0.01$) and produced cutoff distances of 0.52 and 0.49 for 2009 and 2010, respectively. The mean composition of these communities is shown in Fig. 4 as stacked histograms representing percent scatter for each particle type. In 2009 (Fig. 4A–D), Community 3 was overwhelmingly dominated by live *Haslea* sp. cells (Fig. 4C). Community 2 was also dominated by live *Haslea* sp. but had a higher proportion of scatter by other particle types (Fig. 4B). Community 1 had a large proportion of scatter from dead *Haslea* sp. cells (Fig. 4A) and Community 4 had a more even mixture of scatter by different particle types (Fig. 4D). During 2010, phytoplankton communities were not dominated by a single taxon but contained a far more diverse complement of particles with a range of sizes and shapes (Fig. 4E,F). Community 5, although consisting of only 3 samples, was distinctive in composition due to a very high proportion of scatter by dead cells (Fig. 4E). Community 7 contained a high proportion of scatter by large (>100 µm) phytoplankton cells and colonies (Fig. 4G). Community 6 was dominated by non-algal particles (Fig. 4F) and Community 8 had a more even mixture of scatter by all particle types (Fig. 4H).

Mean values and standard deviations of b_p:a_p, c_p slope, a_p slope, and b_{bp}:b_p for each community are shown in Table 1. Results of redundancy analyses for each year (Fig. 5) show the variation of these optical parameters among communities. Permutation tests found the results of both redundancy analyses to be highly significant ($p < 0.005$). In the resulting biplots (Fig. 5), symbols represent samples and symbol shape indicates community membership determined by cluster analyses shown in Fig. 3. The labeled vectors extending from the origin indicate the direction of increase for each optical parameter among all samples. In both years, the a_p slope was correlated with b_p:a_p, and the c_p slope was correlated with

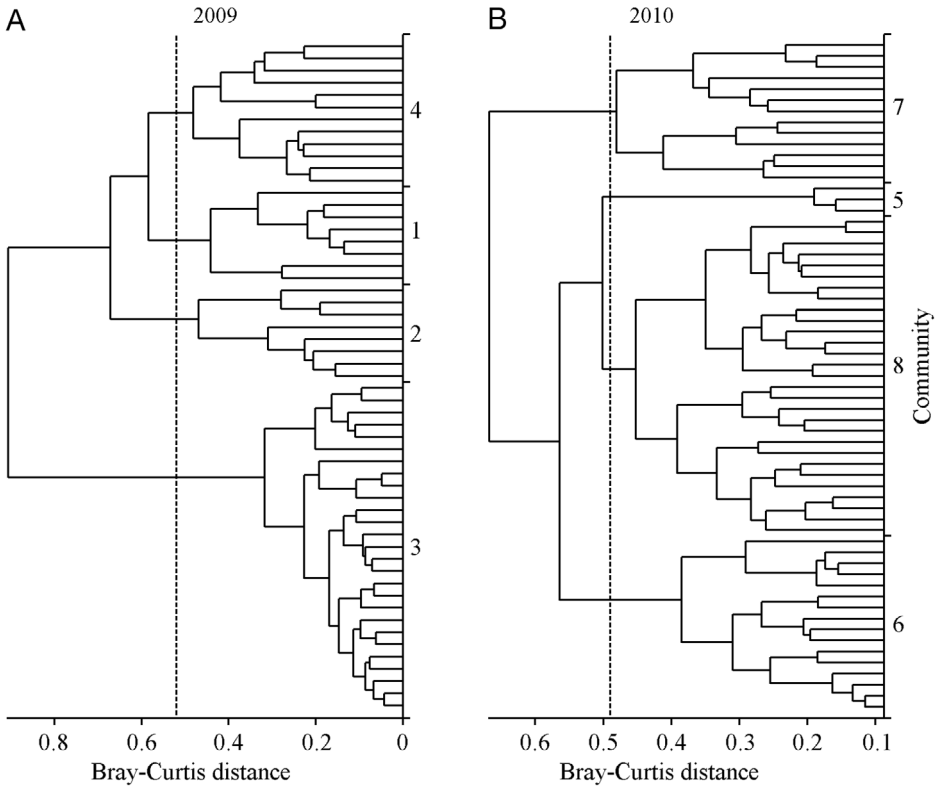

Fig. 3. Dendrograms showing results of cluster analyses for (A) 2009 and (B) 2010, based on particle size–scatter distributions of samples determined with scanning flow cytometry (see Fig. 4). Dashed lines indicate cutoff levels of 0.52 (2009) and 0.49 (2010) determined with similarity profiles ($p < 0.01$)

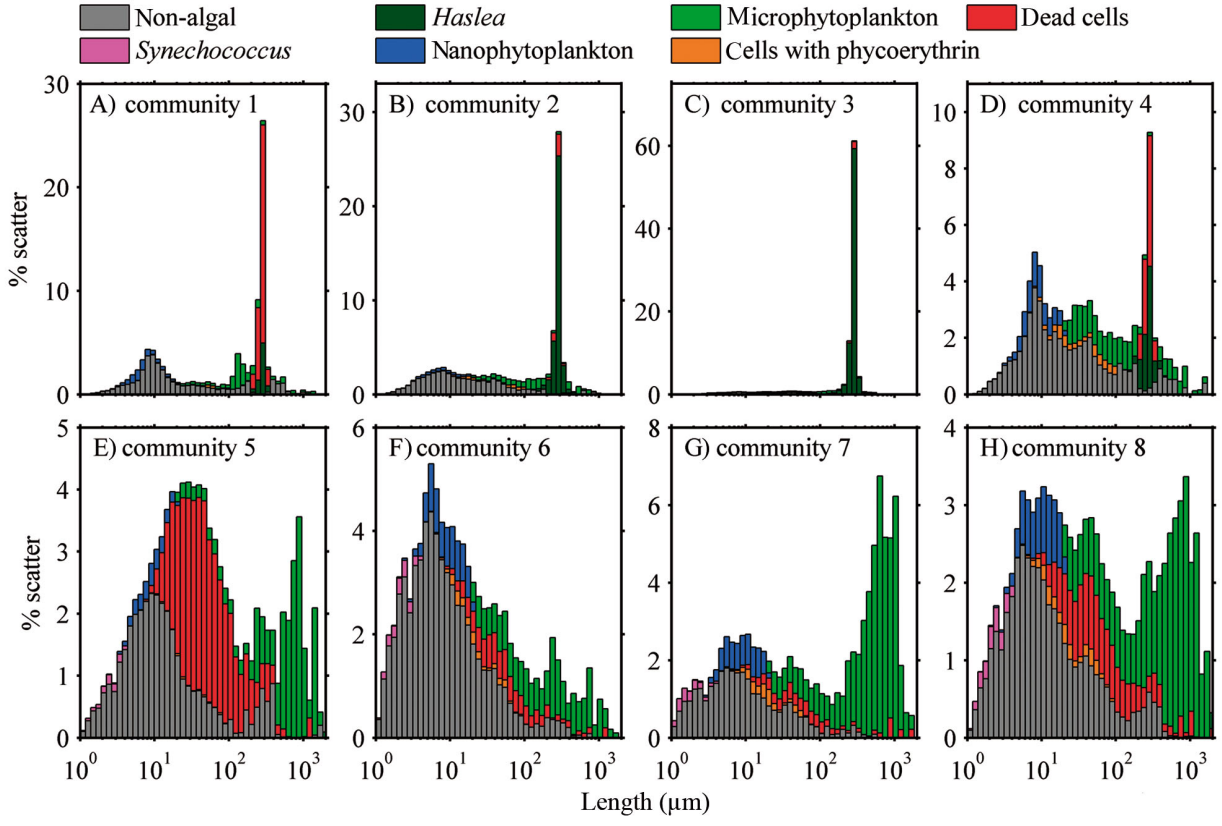

Fig. 4. Mean particulate composition of communities determined with scanning flow cytometry for (A–D) 2009 and (E–H) 2010. Stacked histograms show percentage of total scatter as a function of particle type and length (µm)

Table 1. Number of samples (N) and the mean and standard deviation (SD) of optical parameters for samples in each community

Community	N	b_p:a_p Mean	b_p:a_p SD	c_p slope Mean	c_p slope SD	b_{bp}:b_p Mean	b_{bp}:b_p SD	a_p slope Mean	a_p slope SD
2009									
1	8	16.82	5.33	0.410	0.061	0.0096	0.0012	0.0218	0.0049
2	8	10.35	1.88	0.502	0.132	0.0160	0.0023	0.0131	0.0016
3	27	6.44	0.86	0.281	0.054	0.0112	0.0027	0.0109	0.0012
4	12	18.78	8.78	0.637	0.202	0.0131	0.0032	0.0187	0.0062
2010									
5	3	20.90	4.32	0.091	0.166	0.0070	0.0004	0.0176	0.0037
6	16	10.31	3.49	0.417	0.155	0.0148	0.0045	0.0122	0.0021
7	13	9.21	3.03	0.211	0.157	0.0084	0.0020	0.0120	0.0025
8	29	10.41	4.89	0.241	0.203	0.0082	0.0024	0.0122	0.0033

b_{bp}:b_p. These correlations are most evident in the 2010 analysis. Vector length indicates how well the plotted result represents variation of a particular parameter. In Fig. 5B, for example, the vector representing the c_p slope is relatively short, indicating that the variation of this parameter is not represented as well as other optical parameters in the biplot.

In 2009, Community 1, dominated by dead *Haslea* sp., was found to have high values of b_p:a_p and a_p slope, intermediate c_p slopes, and low values of b_{bp}:b_p (Fig. 5A, Table 1). Samples from Community 2 spanned a range of moderate to high c_p slopes, moderate to high b_{bp}:b_p, and had intermediate values of a_p slope and b_p:a_p. Community 3, dominated by live *Haslea* sp. cells, had low values of c_p slope and a_p slope, low values of b_p:a_p and moderate values of b_{bp}:b_p. Community 4 had high c_p and a_p slopes, high b_p:a_p, and moderate to high vales of b_{bp}:b_p. During 2010, samples in Community 5 had the highest values of b_p:a_p and a_p slopes, low c_p slopes, and low b_{bp}:b_p (Fig. 5B, Table 1). Community 6 had high values of b_{bp}:b_p, high values of c_p slope, and intermediate values of b_p:a_p and a_p slope. Community 7 had moderate to low values of c_p slope and a_p slope, low b_p:a_p, and intermediate values of b_{bp}:b_p. Community 8 spanned a range of intermediate values of all optical parameters.

Comparison of community composition (Fig. 3) with results of redundancy analyses (Fig. 5) and mean community optical parameters (Table 1) shows the influence of particle type on particulate IOPs. During 2009, c_p slopes decreased with the relative amount of scatter by live or dead *Haslea* sp. cells. Also during 2009, the lowest a_p slopes were associated with live *Haslea* sp. cells (Community 3) and the highest a_p slopes were associated with dead *Haslea* sp. cells (Community 1). Conversely, high b_p:a_p was associated with dead *Haslea* sp. cells (Community 1), and low b_p:a_p was associated with live *Haslea* sp. cells (Community 3). However, the b_p:a_p parameter may also have been affected by non-algal particles, as the highest mean values were associated with

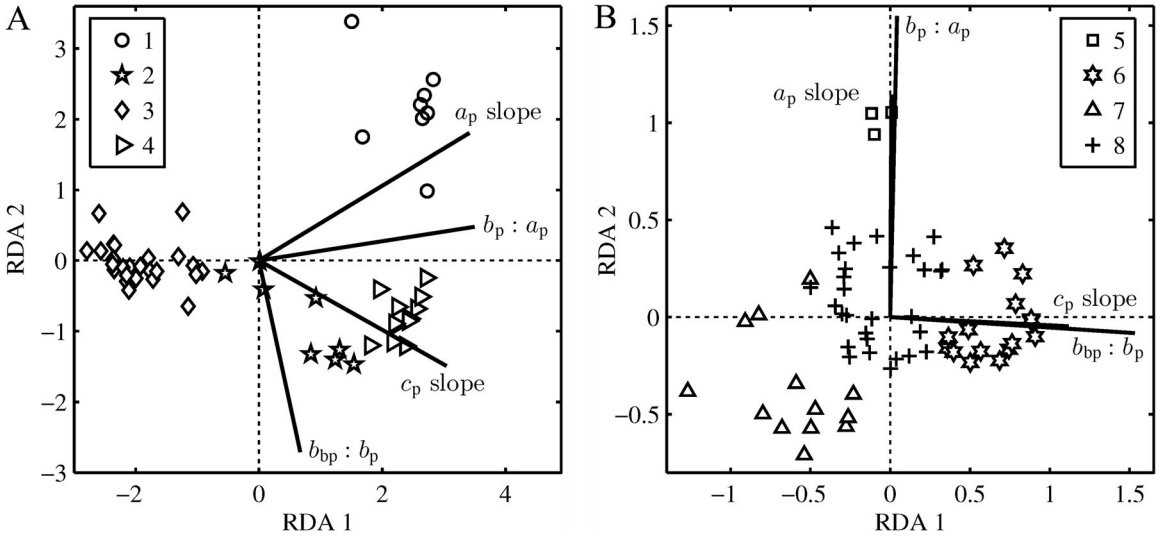

Fig. 5. Biplots showing result of redundancy analysis for (A) 2009 and (B) 2010. Symbols indicate community membership of samples as determined by hierarchical cluster analyses (Fig. 3). Vectors indicate direction of increase for optical parameter values. RDA axes 1 and 2 represent the 2 orthogonal eigenvectors with the largest eigenvalues

Community 4 (Table 1). High values of b_{bp}:b_p were associated with non-algal particles and low b_{bp}:b_p was associated with dead *Haslea* sp. cells. Lower b_{bp}:b_p for Community 1 compared to Community 2 may be attributed to dead *Haslea* sp. cells, as these communities are otherwise similar. Higher b_{bp}:b_p for Community 2 compared to Community 3 is likely due to non-algal particles, since these communities are otherwise similar. During 2010, high c_p slopes were associated with scatter from small, non-algal particles (Community 6), and c_p slopes decreased in association with scatter by large (>100 µm) phytoplankton cells and colonies (Communities 7 and 8). However, the lowest mean c_p slopes were associated with the high scatter from dead cells in Community 5 (Table 1). As in 2009, high b_p:a_p and high a_p slopes were associated with dead cells (Community 5), whereas low b_p:a_p and a_p slopes were associated with large, healthy phytoplankton (Community 7). Also similar to 2009, low values of b_{bp}:b_p were associated with dead cells, and high values of b_{bp}:b_p were associated with scatter from non-algal particles.

Results from both years support 3 general conclusions for East Sound waters. First, communities dominated by large phytoplankton cells and colonies are generally associated with low c_p slope values. This is consistent with previous studies that show c_p slope is a function of the slope of the particle size distribution (Kitchen et al. 1982, Boss et al. 2001). However, the low c_p slope values associated with dead cells during 2010 (Community 5) represent a deviation from this general trend within the context of this study. Second, communities dominated by non-algal particles tend to have higher b_{bp}:b_p, those dominated by live phytoplankton cells have lower b_{bp}:b_p, and those dominated by dead cells have the lowest b_{bp}:b_p values. Third, communities with abundant concentrations of dead phytoplankton are associated with high b_p:a_p ratios and high a_p slopes.

High-resolution autonomous profiles

High-resolution optical data collected with an ORCAS autonomous profiling system were used to infer phytoplankton community characteristics over small scales based on results of discrete sample analyses (Figs. 6 & 7). During both years the ORCAS profiler captured a transition from high-chlorophyll, bloom conditions to waters with low chlorophyll concentrations. In 2009, chlorophyll concentrations were highest below the pycnocline at the start of the high-resolution time series and decreased over time (Fig. 6A). The b_p:a_p ratio was highest near the surface at the beginning of the time series (Fig. 6B). Low b_p:a_p values were found below the pycnocline through the beginning and middle of the time series. The lowest b_p:a_p values were found associated with the pycnocline between 5 and 10 m depth during the middle of the time series. The b_p:a_p parameter was of intermediate value and uniform throughout the water column at the end of the time series. The a_p slope parameter was highest in near-surface waters at the beginning of the time series and decreased with depth below the pycnocline (Fig. 6C). This parameter was lowest throughout the water column near the end of the time series (Fig. 6C). The c_p slope parameter was lowest below the pycnocline and of intermediate value in surface waters at the beginning of the time series (Fig. 6D). Values of c_p slope were high throughout the water column at the end of the time series. The b_{bp}:b_p data collected by the autonomous profiler during 2009 were of poor quality and are not shown.

High-resolution optical data collected in 2010 showed high chlorophyll concentrations in surface waters near the beginning of the time series that decreased over time to form a subsurface maximum between 5 and 10 m depth (Fig. 7A). The b_p:a_p ratio was initially low where chlorophyll concentrations were high, and increased in near-surface waters at the end of the time series (Fig. 7B). Elevated b_p:a_p values in thin layers were associated with the pycnocline between 15 and 20 m on 12 May and between 10 and 15 m on 13 May. The a_p slope parameter was lowest at depth at the start of the time series, moderate to low where chlorophyll concentrations were highest, and generally increased for most of the water column over time, with some lower values remaining in layers between 10 and 20 m (Fig. 7C). The c_p slope parameter was lowest near the surface throughout the time series (Fig. 7D) with strong gradients located along the pycnocline. The b_{bp}:b_p ratio was consistently higher at depth throughout the time series (Fig. 7E).

Based on results of the redundancy analyses, c_p slope values suggest that waters below the pycnocline near the beginning of the time series in 2009 were dominated by large *Haslea* sp. cells. Low b_p:a_p and a_p slopes suggest a low proportion of dead cells in this high-chlorophyll region. In surface waters, moderate c_p slopes, high b_p:a_p, and high a_p slopes suggest abundant dead *Haslea* sp. cells and more abundant small particles. Towards the end of the 2009 time series, high c_p slope and low a_p slope values suggest smaller average particle sizes and a smaller proportion of dead cells. Flow cytometric

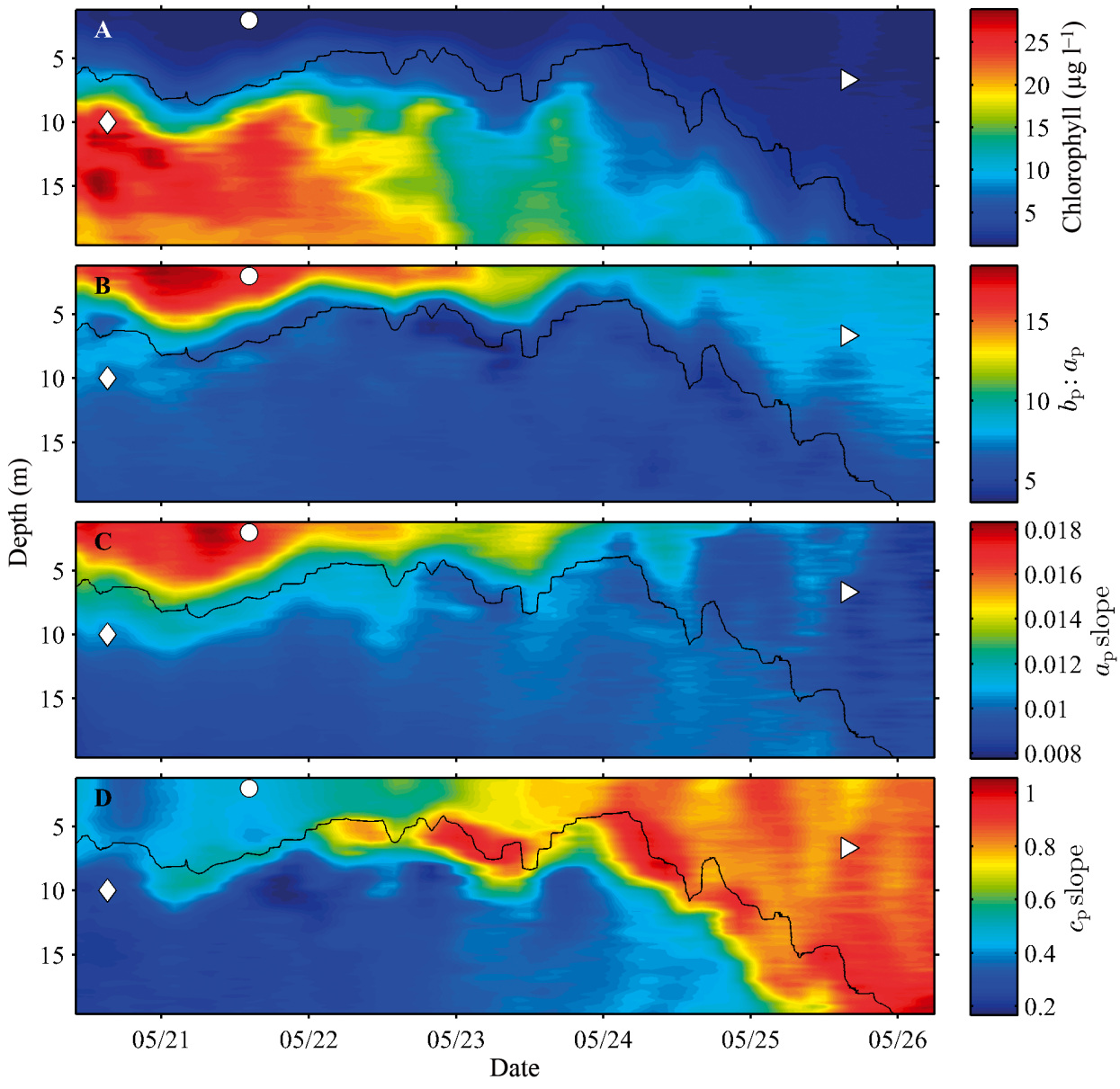

Fig. 6. High-resolution optical data collected during 2009 with the ORCAS autonomous profiler. Symbols indicate location of samples shown in Fig. 8A–C. Black line indicates depth of the pycnocline; Date: mm/dd

analyses of samples collected adjacent to the ORCAS profiler at 3 points during the time series support these optical predictions of particle composition. A sample collected from high-chlorophyll waters below the pycnocline on 20 May was dominated by live *Haslea* sp. (Fig. 8A) with a low proportion of scatter by dead cells (3.03%). There was a greater proportion of scatter by dead cells (10.1%) in near-surface waters on 21 May where b_p:a_p and a_p slopes were high (Fig. 8B). There was also considerably more scatter by small non-algal particles (<10 µm) in these surface waters as predicted by moderate c_p slopes. The sample collected on 25 May, near the end of the time series, contained a higher proportion of scatter by cells in the 10 to 100 µm size range and a lower proportion of scatter (5.5%) by dead *Haslea* sp. cells (Fig. 8C).

The spatial and temporal distribution of c_p slopes in 2010 high-resolution data (Fig. 7D) suggests that large particles dominated in much of the upper portion of the water column throughout the time series, especially after 13 May when chlorophyll concentrations were low. Also throughout the time series, b_{bp}:b_p was higher in near-bottom waters, suggesting non-algal

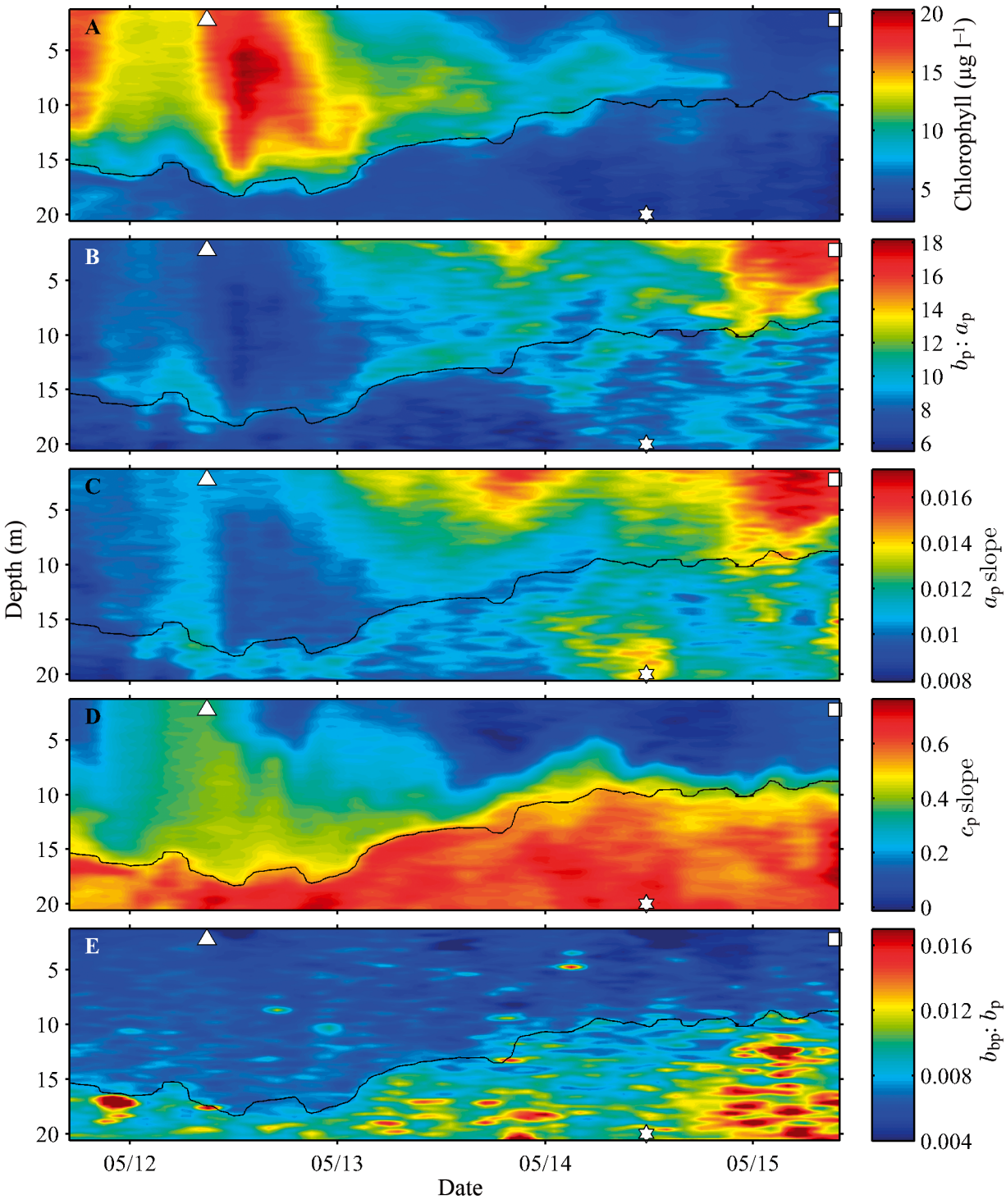

Fig. 7. High-resolution optical data collected during 2010 with the ORCAS autonomous profiler. Symbols indicate location of samples shown in Fig. 8D–F. Black line indicates depth of the pycnocline; Date: mm/dd

particles, possibly re-suspended sediments, are more abundant at depth. High b_p:a_p and a_p slopes in near-surface waters at the end of the time series suggest a high proportion of dead cells. Samples collected close to the ORCAS profiler in 2010 partially support these predictions. A near-surface sample collected on 12 May from the region of high chlorophyll, low b_p:a_p, and moderate a_p slope showed scatter was dominated

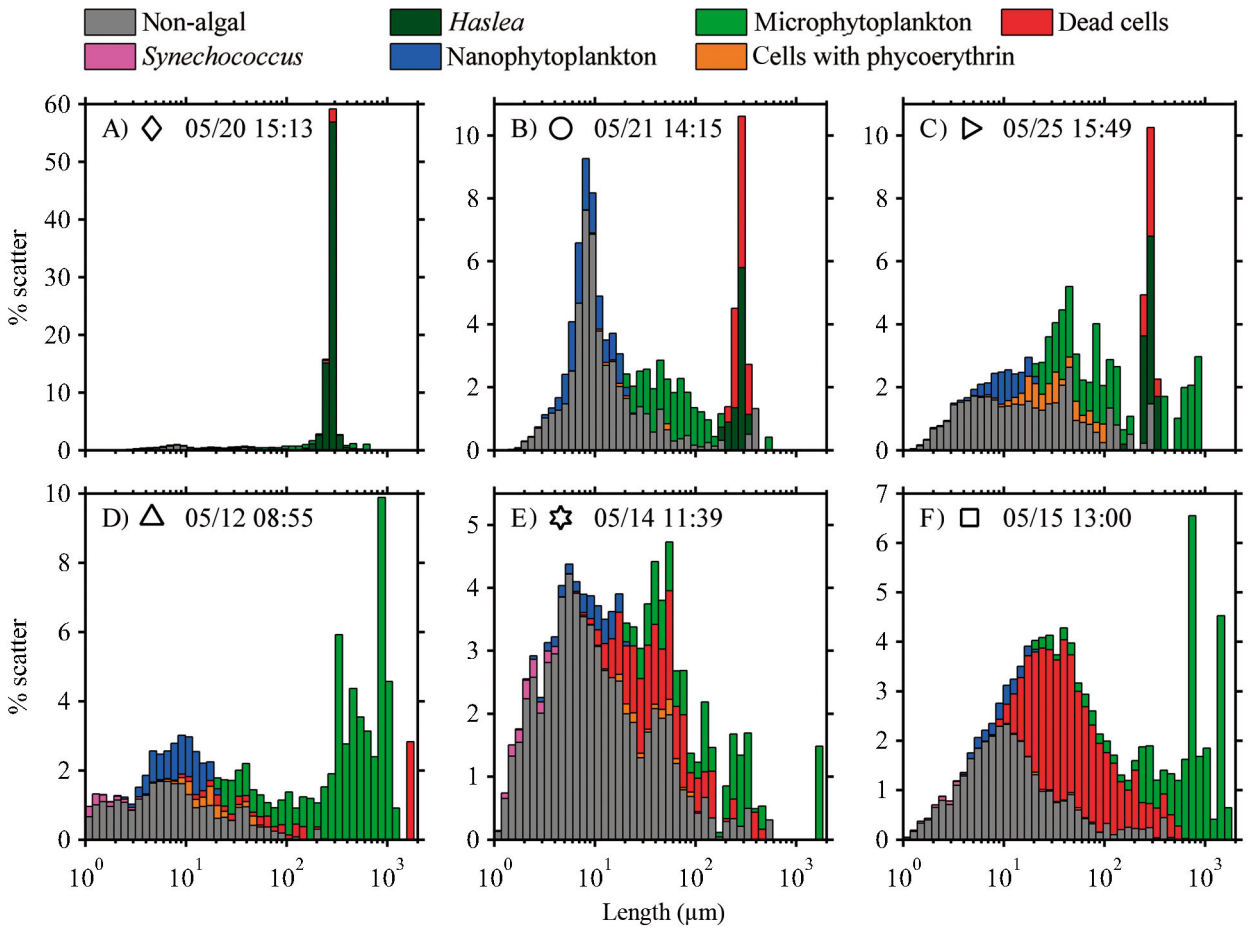

Fig. 8. Composition of individual samples collected near the ORCAS autonomous profiler during (A–C) 2009 and (D–F) 2010 shown as percent scatter determined by scanning flow cytometry. Symbols correspond to sample locations in Figs. 6 & 7 and to the communities they most resemble as in Fig. 5. Date: mm/dd

by large (>100 µm) phytoplankton cells and colonies (Fig. 8D). A sample collected from ~20 m depth on 14 May showed scatter dominated by non-algal particles (Fig. 8E). A sample collected near the surface at the end of the time series showed considerable scatter from dead cells (Fig. 8F). Although c_p slope for waters dominated by phytoplankton colonies >100 µm in size was lower than that for waters dominated by small non-algal particles, the lowest c_p slopes were associated with abundant dead cells in the 10 to 100 µm size range. This is contrary to the normal positive correlation between c_p slope and the relative abundance of large particles (Kitchen et al. 1982, Boss et al. 2001), but in agreement with results from previous sample analyses that showed low c_p slopes associated with dead cells (Community 5, Table 1). For the large diatom colonies that were found in East Sound during the study in 2010, morphology may play an important role in determining their scattering characteristics and the c_p slope parameter.

DISCUSSION

This study compared phytoplankton and non-algal particle characteristics determined with scanning flow cytometry to *in situ* measurements of particulate IOPs over small scales. The results show a strong influence of phytoplankton type, size, and pigment content on the spectral shape and relative magnitude of a_p, c_p, and b_p coefficients. Variation in phytoplankton community composition, primarily driven by the relative abundance of large (>200 µm) diatom cells and colonies, determined c_p slope. However, it appears the complex morphology of some large colonies resulted in higher c_p slopes than would be expected based on their size as measured with the CytoSense scanning flow cytometer. Phytoplankton cell death and subsequent loss of chlorophyll increased b_p:a_p and a_p slopes. In addition, the relative abundance of non-algal particles primarily determined b_{bp}:b_p. These results demonstrate the ability of

optical parameters to reveal variation of phytoplankton community structure and function with high resolution over ecologically critical, small spatial and temporal scales in the ocean.

Results were similar for 2 very different phytoplankton communities. In 2009, suspended particles in East Sound were dominated by a single diatom taxon in the genus *Haslea*. Its relative abundance throughout the water column over time was inversely correlated with the c_p slope parameter. The death of this population was associated with dramatic increases in b_p:a_p and a_p slope as cellular pigment content changed and the proportion of empty frustules increased. Increases in b_p:a_p are likely due to a decrease in absorption by dead cells through loss of chlorophyll and an increase in non-algal particulate material such as cell debris and bacteria. Increases in a_p slope may be associated with a relative increase in absorption by photoprotective carotenoids (Eisner et al. 2003), or with changes in pigment packaging as cells die (Duyens 1956, Kirk 1975, Ciotti et al. 2002). During a previous study in Monterey Bay, high a_p slopes were associated with dense populations of large cells with high pigment packaging (M. McFarland unpubl.), while in East Sound it seems more likely that changes in pigment characteristics as cells died determined changes in a_p slope.

Although the phytoplankton community contained very different taxa and was far more diverse in 2010, similar results were found. With the exception of Community 5, the abundance of large colonial diatoms (*Chaetoceros socialis* in particular) was inversely related to the c_p slope. As these cells died, b_p:a_p and the a_p slope increased. In this case, dead and dying cells covered a range of sizes as large colonies fell apart into single cells or short chains. Contrary to expectations, these smaller dead cells and colony fragments were associated with the lowest c_p slopes (Table 1). This result may be owing to the morphology of large intact *C. socialis* colonies, which are several hundred micrometers in size, composed of curving, intertwined chains of cells, and held together with multiple long, thin, siliceous setae (Fig. 1C). This open structure may scatter light in a similar way to populations of smaller, discrete particles, resulting in higher c_p slopes than would be expected from theoretical predictions based on the assumption that particles are solid spheres or ellipsoids (e.g. Mie theory) with diameters equivalent to lengths measured by scanning flow cytometry. Such optical behavior may be attributed to a lack of interaction among light waves scattered from individual components (e.g. setae, frustules) of the colony due to their physical separation in space. Large porous aggregates with a low fraction of solid material, such as *C. socialis* colonies, can have higher than expected mass-specific attenuation (Boss et al. 2009) and may also have higher c_p slopes. Disintegration of *C. socialis* colonies as cells died and possible aggregation of colony fragments may have resulted in particles with higher solid fractions and c_p slopes lower than for healthy, intact colonies.

In both years, optical data proved to be an effective tool for visualizing changes in phytoplankton community characteristics with high resolution over small spatial and temporal scales. Autonomous *in situ* measurements from the ORCAS profiler enabled visualization of small-scale features and important ecological processes that would have been otherwise very difficult to detect. During 2009, dead *Haslea* cells accumulated near the surface rather than sinking. This was visually confirmed by a distinctive surface slick seen throughout the sound at the termination of the bloom. Dead *Haslea* sp. cells may have been positively buoyant due to intracellular accumulation of lipids. Also during 2009, the depth of the pycnocline corresponded to a minimum in b_p:a_p values and high c_p slopes (Fig. 6). This suggests that the thin transition region between low- and high-density waters contained very few dead cells or large particles. During 2010, the depth of the pycnocline at times corresponded to elevated b_p:a_p values. This suggests that dying cells were settling out of surface waters and accumulating at the interface between low- and high-density waters (Alldredge et al. 2002), a process that may have implications for biogeochemical cycling on a global scale. These small-scale features would not have been visible by looking only at measures of total phytoplankton abundance such as chlorophyll absorption or fluorescence.

The strong relationships found between measured particles and IOPs suggest that our methods have accurately measured the majority of optically important particulate material. However, it is also possible that very small particles below the detection limit of the flow cytometer (0.2 to 2 µm), such as bacteria, viruses, and colloids, also contributed to some of the optical variation seen in East Sound. While these particles are very small, they are also very abundant and their impact on bulk optical properties remains poorly understood, primarily due to the difficulty of measuring their abundance *in situ*. If distributions of these unmeasured particles were correlated with larger measured particles, their optical significance could have been underestimated. This may be likely in the case of bacteria and viruses whose abundance

could be directly associated with dead and dying phytoplankton. Alternatively, variation in the abundance of very small, unmeasured particles likely contributed substantially to the optical variation seen within each of our communities. Particles smaller than 0.2 µm would have been included in our measurements of dissolved material and therefore should not have had an impact on our analyses.

This study provides new evidence that certain morphological and physiological characteristics of phytoplankton can be derived from *in situ* optical measurements to study ecological patterns and processes in the ocean, with high resolution. Currently, the ecological dynamics of phytoplankton communities over small spatial and temporal scales are poorly understood. Processes at these scales, however, are critical to the ecology of individual species and populations, and to the function of marine ecosystems. Small-scale structure is often observed as high-biomass layers and patches that have distinct taxonomic composition (Rines et al. 2002, McManus et al. 2003, Rines et al. 2010). This suggests that communities and overall marine ecosystem structure are shaped by responses of species to different environmental conditions. The resulting ecological heterogeneity may be important for generating and maintaining diversity and to rates of primary production, carbon export, and transfers of energy through ocean food webs. Use of optical techniques as demonstrated here can provide the tools necessary to greatly enhance our understanding of phytoplankton ecology at small scales. High-resolution mapping and monitoring of phytoplankton abundance and characteristics enables localization of growth and mortality with respect to light intensity, nutrient concentrations, and zooplankton grazer abundance at the scales important to population dynamics. Phytoplankton characteristics and community dynamics can also be clearly linked to physical water column structure and hydrographic processes such as upwelling, stratification, mixing, or lateral intrusion to explain observed patterns of distribution and abundance. A better understanding of mortality and bloom senescence is particularly important in the context of global climate change since, over broader scales, these processes have a direct impact on the biological pumping of carbon to deep ocean waters where it can be sequestered for centuries or longer (Smetacek et al. 2012).

Results show the particulate optical properties of natural phytoplankton communities clearly vary with biologically important morphological and physiological characteristics of cells and colonies. However, the relationship between cellular characteristics and optical properties can be influenced by multiple factors, and optical data may be difficult to interpret without additional information. Simultaneous biological or chemical analyses of discrete samples, therefore, may be required to accurately determine ecological patterns and processes from *in situ* optical measurements.

Acknowledgements. We are grateful for the help and collaboration of George Dubelaar, and for the constructive comments from several anonymous reviewers that helped to improve the paper. We also thank the Office of Narval Research for their commitment to our research program. This work was supported by ONR grants N000140410275 (J.R.), N000140811217 (P.D., J.S., and J.R.), and N000140910492 (P.D., J.R., and J.S.).

LITERATURE CITED

Ackleson SG, Spinrad RW, Yentsch CM, Brown J, Korjeff-Bellows W (1988) Phytoplankton optical properties: flow cytometric examinations of dilution-induced effects. Appl Opt 27:1262–1269

Alldredge AL, Cowles TJ, MacIntyre S, Rines JEB and others (2002) Occurrence and mechanisms of formation of a dramatic thin layer of marine snow in a shallow Pacific fjord. Mar Ecol Prog Ser 233:1–12

Babin M, Stramski D, Ferrari GM, Claustre H, Bricaud A, Obolensky G, Hoepffner N (2003) Variations in the light absorption coefficients of phytoplankton, non-algal particles, and dissolved organic matter in coastal waters around Europe. J Geophys Res C 108:3211

Babin M, Cullen JJ, Roesler CS, Donaghay PL and others (2005) New approaches and technologies for observing harmful algal blooms. Oceanography 18:210–227

Benoit-Bird KJ, Cowles TJ, Wingard CE (2009) Edge gradients provide evidence of ecological interactions in planktonic thin layers. Limnol Oceanogr 54:1382–1392

Bjørnsen PK, Nielsen TG (1991) Decimeter scale heterogeneity in the plankton during a pycnocline bloom of *Gyrodinium aureolum*. Mar Ecol Prog Ser 73:263–267

Boss E, Twardowski MS, Herring S (2001) Shape of the particulate beam attenuation spectrum and its inversion to obtain the shape of the particulate size distribution. Appl Opt 40:4885–4893

Boss E, Slade W, Hill P (2009) Effect of particulate aggregation in aquatic environments on the beam attenuation and its utility as a proxy for particulate mass. Opt Express 17:9408–9420

Bricaud A, Morel A, Prieur L (1983) Optical efficiency factors of some phytoplankters. Limnol Oceanogr 28:816–832

Bricaud A, Claustre H, Ras J, Oubelkheir K (2004) Natural variability of phytoplanktonic absorption in oceanic waters: influence of the size structure of algal populations. J Geophys Res C 109:C11010, doi:10.1029/2004JC002419

Cassie RM (1963) Microdistribution of plankton. Oceanogr Mar Biol Annu Rev 1:223–252

Ciotti AM, Lewis MR, Cullen JJ (2002) Assessment of the relationships between dominant cell size in natural phytoplankton communities and the spectral shape of

the absorption coefficient. Limnol Oceanogr 47:404–417
Clarke KR, Somerfield PJ, Gorley RN (2008) Testing of null hypotheses in exploratory community analyses: similarity profiles and biota-environment linkage. J Exp Mar Biol Ecol 366:56–69
Cowles TJ, Desiderio RA (1993) Resolution of biological microstructure through *in situ* fluorescence emission spectra. Oceanography 6:105–111
Cowles TJ, Desiderio RA, Carr ME (1998) Small-scale planktonic structure: persistence and trophic consequences. Oceanography 11:4–9
Dekshenieks MM, Donaghay PL, Sullivan JM, Rines JEB, Osborn TR, Twardowski MS (2001) Temporal and spatial occurrence of thin phytoplankton layers in relation to physical processes. Mar Ecol Prog Ser 223:61–71
Derenbach JB, Astheimer H, Hansen HP, Leach H (1979) Vertical microscale distribution of phytoplankton in relation to the thermocline. Mar Ecol Prog Ser 1:187–193
Donaghay PL (2003) Profiling systems for understanding the dynamics and impacts of thin layers of harmful algae in stratified coastal waters. In: Proc 4th Irish Marine Biotoxin Science Workshop. Marine Institute, Renvyle, p 44–53
Donaghay PL, Osborn TR (1997) Toward a theory of biological-physical control of harmful algal bloom dynamics and impacts. Limnol Oceanogr 42:1283–1296
Donaghay PL, Rines HM, Sieburth JM (1992) Simultaneous sampling of fine scale biological, chemical, and physical structure in stratified waters. Arch Hydrobiol 36:97–108
Durham WM, Stocker R (2012) Thin phytoplankton layers: characteristics, mechanisms, and consequences. Annu Rev Mar Sci 4:177–207
Duyens LNM (1956) The flattening of the absorption spectrum of suspensions, as compared to that of solutions. Biochim Biophys Acta 19:1–12
Eisner LB, Cowles TJ (2005) Spatial variations in phytoplankton pigment ratios, optical properties, and environmental gradients in Oregon coast surface waters. J Geophys Res C 110:C10S14, doi:10.1029/2004JC002614
Eisner LB, Twardowski MS, Cowles TJ, Perry MJ (2003) Resolving phytoplankton photoprotective: photosynthetic carotenoid ratios on fine scales using *in situ* spectral absorption measurements. Limnol Oceanogr 48:632–646
Green RE, Sosik HM, Olson RJ (2003) Contributions of phytoplankton and other particles to inherent optical properties in New England continental shelf waters. Limnol Oceanogr 48:2377–2391
Greer AT, Cowen RK, Guigand CM, McManus MA, Sevadjian JC, Timmerman AHV (2013) Relationships between phytoplankton thin layers and the fine-scale vertical distributions of two trophic levels of zooplankton. J Plankton Res 35:939–956
Guillard RRL, Hargraves PE (1993) *Stichochrysis immobilis* is a diatom, not a chrysophyte. Phycologia 32:234–236
Hanson AK, Donaghay PL (1998) Micro- to fine-scale chemical gradients and layers in stratified coastal waters. Oceanography 11:10–17
Haury LR, McGowan JA, Wiebe PH (1978) Patterns and processes in the time-space scales of plankton distributions. In: Steele JH (ed) Spatial pattern in plankton communities. Plenum Press, New York, NY, p 277–327
Holliday DV, Donaghay PL, Greenlaw CF, McGehee DE, McManus MM, Sullivan JM, Miksis JL (2003) Advances in defining fine- and micro-scale pattern in marine plankton. Aquat Living Resour 16:131–136
Holliday DV, Donaghay PL, Greenlaw CF, Napp JM, Sullivan JM (2009) High-frequency acoustics and bio-optics in ecosystems research. ICES J Mar Sci 66:974–980
Iturriaga R, Siegel DA (1989) Microphotometric characterization of phytoplankton and detrital absorption properties in the Sargasso Sea. Limnology and Oceanography:1706–1726
Jones DL (2012) The fathom toolbox for MATLAB: multivariate ecological and oceanographic data analysis. College of Marine Science, University of South Florida, St. Petersburg, FL
Kirk JTO (1975) A theoretical analysis of the contribution of algal cells to the attenuation of light within natural waters. I. General treatment of suspensions of pigmented cells. New Phytol 75:11–20
Kitchen JC, Zaneveld JRV, Pak H (1982) Effect of particle size distribution and chlorophyll content on beam attenuation spectra. Appl Opt 21:3913–3918
McManus MA, Alldredge AL, Barnard AH, Boss E and others (2003) Characteristics, distribution and persistence of thin layers over a 48 hour period. Mar Ecol Prog Ser 261:1–19
Menden-Deuer S (2008) Spatial and temporal characteristics of plankton-rich layers in a shallow, temperate fjord. Mar Ecol Prog Ser 355:21–30
Morel A, Bricaud A (1986) Inherent optical properties of algal cells including picoplankton: theoretical and experimental results. In: Platt T, Li WKW (eds) Photosynthetic picoplankton. Department of Fisheries and Oceans, Ottawa, p 521–559
Nielsen TG, Kiørboe T, Bjørnsen PK (1990) Effects of a *Chrysochromulina polylepis* subsurface bloom on the planktonic community. Mar Ecol Prog Ser 62:21–35
Oksanen J, Blanchet FG, Kindt R, Legendre P and others (2013) vegan: community ecology package. R package version 2.0-7. http://CRAN.R-project.org/package=vegan
Peperzak L (2006) Below the Kolmogorov scale: the nonturbulent sex life of phytoplankton. Afr J Mar Sci 28: 261–264
Reynolds C (2006) Ecology of phytoplankton. Cambridge University Press, Cambridge
Rines JEB, Donaghay PL, Dekshenieks MM, Sullivan JM, Twardowski MS (2002) Thin layers and camouflage: hidden *Pseudo-nitzschia* spp. (Bacillariophyceae) populations in a fjord in the San Juan Islands, Washington, USA. Mar Ecol Prog Ser 225:123–137
Rines JEB, McFarland MN, Donaghay PL, Sullivan JM (2010) Thin layers and species-specific characterization of the phytoplankton community in Monterey Bay, California, USA. Cont Shelf Res 30:66–80
Röttgers R, McKee D, Woźniak SB (2013) Evaluation of scatter corrections for ac-9 absorption measurements in coastal waters. Methods Oceanogr 7:21–39
Sathyendranath S, Lazzara L, Prieur L (1987) Variations in the spectral values of specific absorption of phytoplankton. Limnol Oceanogr 32:403–415
Sieburth JMcN, Donaghay PL (1993) Planktonic methane production and oxidation within the algal maximum of the pycnocline: seasonal fine-scale observations in an anoxic estuarine basin. Mar Ecol Prog Ser 100:3–15
Smayda TJ, Reynolds CS (2001) Community assembly in marine phytoplankton: application of recent models to harmful dinoflagellate blooms. J Plankton Res 23: 447–461

Smetacek V, Klaas C, Strass VH, Assmy P and others (2012) Deep carbon export from a Southern Ocean iron-fertilized diatom bloom. Nature 487:313–319

Sosik HM, Green RE, Pegau WS, Roesler CS (2001) Temporal and vertical variability in optical properties of New England shelf waters during late summer and spring. J Geophys Res 106:9455–9472

Spinrad RW, Yentsch CM (1987) Observations on the intra- and interspecific single cell optical variability of marine phytoplankton. Appl Opt 26:357–362

Stemmann L, Boss E (2012) Plankton and particle size and packaging: from determining optical properties to driving the biological pump. Annu Rev Mar Sci 4: 263–290

Stramski D, Morel A (1990) Optical properties of photosynthetic picoplankton in different physiological states as affected by growth irradiance. Deep-Sea Res A 37: 245–266

Stramski D, Reynolds RA (1993) Diel variations in the optical properties of a marine diatom. Limnol Oceanogr 38: 1347–1364

Sullivan JM, Swift E (2003) Effects of small-scale turbulence on net growth rate and size of ten species of marine dinoflagellates. J Phycol 39:83–94

Sullivan JM, Twardowski MS, Donaghay PL, Freeman SA (2005) Use of optical scattering to discriminate particle types in coastal waters. Appl Opt 44:1667–1680

Sullivan JM, Twardowski MS, Zaneveld JRV, Moore CM, Barnard AH, Donaghay PL, Rhoades B (2006) Hyperspectral temperature and salt dependencies of absorption by water and heavy water in the 400–750 nm spectral range. Appl Opt 45:5294–5309

Sullivan JM, Donaghay PL, Rines JEB (2010a) Coastal thin layer dynamics: consequences to biology and optics. Cont Shelf Res 30:50–65

Sullivan JM, Van Holliday D, McFarland M, McManus MA and others (2010b) Layered organization in the coastal ocean: an introduction to planktonic thin layers and the LOCO project. Cont Shelf Res 30:1–6

Sullivan JM, Twardowski MS, Zaneveld JRV, Moore CC (2013) Measuring optical backscattering in water. In: Kokhanovsky AA (ed) Light scattering reviews 7. Springer, Berlin, p 189–224

Twardowski MS, Sullivan JM, Donaghay PL, Zaneveld JRV (1999) Microscale quantification of the absorption by dissolved and particulate material in coastal waters with an ac-9. J Atmos Ocean Tech 16:691–707

Twardowski MS, Boss E, Macdonald JB, Pegau WS, Barnard AH, Zaneveld JRV (2001) A model for estimating bulk refractive index from the optical backscattering ratio and the implications for understanding particle composition in case I and case II waters. J Geophys Res 106:14129–14142

Zaneveld JRV, Kitchen JC, Moore CC (1994) Scattering error correction of reflecting-tube absorption meters. Proc SPIE 2258:44–55

Zuur AF, Ieno EN, Smith GM (2007) Analysing ecological data. Springer Verlag, New York, NY

Editorial responsibility: Steven Lohrenz, New Bedford, Massachusetts, USA

Submitted: October 13, 2014; Accepted: April 22, 2015
Proofs received from author(s): June 16, 2015